Research Article Vol. 33, No. 26 / 29 Dec 2025 / Optics Express 54747
Optics EXPRESS

High-power heterogeneously integrated mode-locked laser enabled by a booster amplifier

STIJN POELMAN,* TOM REEP, MAXIMILIEN BILLET, AND BART KUYKEN

Photonics Research Group, INTEC, Ghent University - imec, 9052 Ghent, Belgium
stijn.poelman@ugent.be

Abstract: Integrated mode-locked lasers have emerged as promising comb sources over recent years, with the prospect of their use in many applications such as telecommunications, lidar and dual-comb spectroscopy. While these integrated implementations have the advantage of a smaller footprint and cost compared to their table-top counterparts, the lower output powers have been a significant downside for their use in applications. Here, we demonstrate a heterogeneously integrated III/V-on-silicon nitride mode-locked laser with a 3 GHz repetition frequency. The heterogeneous integration is enabled by micro-transfer printing, which is a versatile approach utilized not only for the integration of the III/V semiconductor optical amplifier, but also a silicon interposer coupon. This two-step micro-transfer printing approach is used to integrate a mode-locked laser combined with a booster amplifier, placed at one of the mode-locked laser outputs, where the output power is amplified by up to 10.5 dB, enabling average powers of 11 dBm on-chip.

© 2025 Optica Publishing Group under the terms of the Optica Open Access Publishing Agreement

1. Introduction

Mode-locked lasers (MLLs) are able to generate short pulses with a fixed repetition frequency, which is interesting for a rapidly expanding number of applications such as telecommunication [1], spectroscopy [2,3] and ranging [4,5]. Research has been moving away from the bulky and expensive solid-state and fiber-based laser sources, as miniaturization and energy efficiency are becoming increasingly crucial. Photonic integrated circuits (PICs) have been key enablers of this search for low-cost, scalable and compact implementations of optical components, making use of the existing complementary metal-oxide semiconductor (CMOS) facilities. Mode-locked lasers in particular are interesting comb sources for applications requiring low repetition rates, such as (dual-comb) spectroscopy [2]. Monolithic mode-locked laser have enabled several demonstrations of miniaturized, high-power comb sources [6–8] but are constrained to higher repetition frequencies and exhibit limitations in noise performance. One of the most promising approaches recently has been to combine a low-loss passive platform with a III/V gain material through hybrid or heterogeneous integration. Hybrid integration allows to decouple the design of the III/V active chip and the low loss passive chip and has led to demonstrations such as a high pulse energy mode-locked laser in nanophotonic lithium niobate and silicon nitride [9,10]. Heterogeneous integration on the other hand still enables single-chip devices, while combining active and passive materials. Silicon nitride platforms have been established as a very promising solution for the passive platform, offering low propagation losses (<1 dB/m) over a wide transparency range at wafer-scale level [11]. Furthermore the negligible two-photon absorption at telecom wavelengths and low thermo-optic coefficient are strong advantages compared to the previously standard silicon passive platforms (SiN: 2.45×10^{-5} K^{-1}, Si: 1.86×10^{-4} K^{-1} [12]).

A major challenge lies in the efficient evanescent coupling between the low-index passive SiN platform and high-index III/V materials, due to fabricational limitations of the latter. Amorphous

#581535 https://doi.org/10.1364/OE.581535
Journal © 2025 Received 13 Oct 2025; revised 28 Nov 2025; accepted 3 Dec 2025; published 22 Dec 2025

Optics EXPRESS

silicon (a-Si) and crystalline silicon (c-Si) intermediate layers, including low-loss adiabatic coupling sections, have been successfully incorporated to create III/V-on-SiN amplifiers [13], continuous wave (CW) lasers [14–16] and mode-locked lasers [17–19]. Different heterogeneous integration approaches have been taken towards the exploration of on-chip CW lasers and mode-locked lasers, including bonding [14,15,20] and micro-transfer printing [13,16–19]. While bonding is the most mature technology, micro-transfer printing is quickly gaining traction as it offers attractive advantages including efficient material use, no requirement for III/V post-processing and remarkable flexibility for integration of a myriad of thin-film materials onto different passive platforms [21,22]. It also facilitates 3D integration in a recess, which is a key feature for compatibility with mature silicon photonics platforms including metals.

This integration approach was used in recent demonstrations of III/V-on-SiN mode-locked lasers, to create a record-low repetition rate of 755 MHz with average waveguide-coupled power of 0.125 mW and corresponding 0.16 pJ pulse energy using a SiN-on-Si-on-insulator [18]. In another approach, an amorphous silicon intermediate layer was used to create a 3 GHz III/V-on-SiN mode-locked laser exhibiting 6 mW output power with corresponding 2 pJ pulse energy [17]. While these heterogeneous demonstrations provide superior performance in terms of low repetition rates, optical bandwidths and linewidths compared to monolithic comb sources, their main drawback comes from the currently attainable optical output powers, which are significantly lower than their monolithic counterparts [23].

In this work, we fully capitalize on the versatility of micro-transfer printing, for the integration of both a III/V semiconductor optical amplifier (SOA) and the intermediate silicon layer in a two-step integration approach. Furthermore, this method is employed for the mode-locked laser as well as for a booster amplifier enabling us to exceed the output powers previously reached using heterogeneously integrated solutions, up to 11 dBm average waveguide-coupled power, with minimal effect on the comb properties.

2. Design

Figure 1 shows an artistic rendition of the mode-locked laser device presented in this work. The mode-locked laser structure described in this work has a symmetric ring topology, creating a colliding-pulse mode-locked laser in which two pulses are counter-propagating [18,24,25]. Compared to alternatives, such as Fabry-Perot cavities, a ring mode-locked laser requires no mirrors, which could introduce unwanted spectral shaping. A mode-locked laser was designed for a 3 GHz repetition rate, with the addition of two 2-cm-long SiN waveguide spirals. The waveguide losses of this platform were measured to be around 0.3 dB/cm. Centrally placed

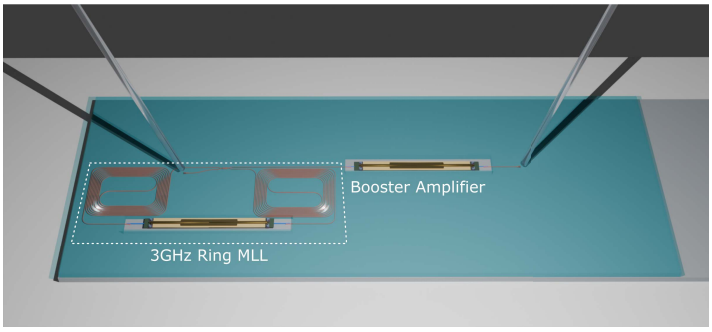

Fig. 1. Artistic render of the ring mode-locked laser with booster amplifier, where III/V SOAs are integrated into local recess openings in the top cladding. Light is captured from the MLL and booster outputs using grating couplers and cleaved single-mode fibers.

Optics EXPRESS

in the laser cavity is a 2.5 mm long multi-quantum well semiconductor optical amplifier. The saturable absorber required for this type of mode-locked laser is created by reverse biasing a 100 μm long isolated section of the III-V amplifier [26]. As such the amplifier consists of three electrically isolated sections, two of which are forward biased to achieve gain, and the third, centrally placed, is reverse biased to serve as the saturable absorber [27]. An 85/15 multimode interferometer was used to couple light out of the laser device. The laser cavity is connected through the cross-coupling (85%), while the through-coupled connections (15%) couple light out of the cavity.

To increase the power of this comb laser, another semiconductor optical amplifier was introduced after one of these output waveguides, while the other is routed straight to an output grating coupler, to serve as reference output. For both sides grating couplers are used to couple the light into cleaved single-mode fibers, with a measured insertion loss of 6 dB at a wavelength of 1530 nm.

3. Fabrication

The low-loss waveguides used to create this 3 GHz mode-locked laser are patterned in a passive platform with 300 nm silicon nitride on a 3.3 μm buried oxide layer using electron beam lithography and reactive ion etching. On top of these passive circuits a 35-nm-thick aluminum oxide layer is deposited using atomic layer deposition, as a necessary etch stop layer for subsequent etching steps. The chip is then cladded with a 2-μm-thick oxide cladding, deposited using inductively coupled plasma chemical vapor deposition.

The heterogeneous integration of the III/V amplifier is done through micro-transfer printing [28]. In this integration method, thin-film coupons, which are preprocessed and suspended on their source wafer are picked up using an elastomer stamp and printed on the target substrate. This is a versatile approach which has been used to demonstrate the integration of not only semiconductor optical amplifiers, but also lithium niobate modulators [21], uni-travelling carrier photodiodes [22] and magneto-optical films [29] on a wide variety of target platforms. Furthermore, contrary to alternatives such as wafer-bonding integration of these devices can be done inside local recesses, which is convenient for the integration on low-loss commercial platforms relying on a thick oxide cladding [30]. There is also great potential for massively parallel integration on a wafer scale with submicrometer precision and yields of over 99.9% [31].

In this work, micro-transfer printing is employed not only for integration of the III/V amplifier, but also a silicon interposer layer, required to bridge the refractive index gap between the low-index silicon nitride and the high-index InP-based SOA. To facilitate this efficient coupling, the thick top oxide cladding needs to be removed locally, as such that the silicon coupon and amplifier can be integrated closely on top of the passive SiN waveguide. This is done with a photolithography and reactive ion etching step, creating 3 mm x 250 μm local recesses. For the interposer layer, 400-nm-thin unpatterned silicon coupons are fabricated. After definition of the 2.9 mm x 80 μm coupons, photoresist is used to encapsulate the coupons and to create tethers to the substrate. Hydrofluoric acid is used to underetch the buried oxide layer and create suspended coupons, supported only by the photoresist tethers. A 70-nm-thin layer of benzocyclobutene (BCB) is spincoated as an adhesive layer on the target chip, after which the silicon coupons are picked up from their source sample using a polymer stamp, and printed on the target. The photoresist encapsulation is subsequently removed using acetone rinsing and oxygen plasma cleaning. A curing step at 280 °C ensures the formation of a strong and durable bond. Alignment accuracies up to 500 nm 3σ can be reached for this integration method, however in this approach with the unpatterned coupons, alignment is not critical. An alternative strategy was investigated in [30], where the tapers are created in the pre-processed coupons, removing the need for an etch stop layer. That approach does however rely on the transfer-printing accuracy and struggles with the reliable transfer of the fragile taper structures. Here, the taper structures are defined

Optics EXPRESS

after transfer-printing by means of electron beam lithography and inductively-coupled plasma (ICP) etching. As such the alignment accuracy is determined by that of the electron beam patterning, which has a 100 nm accuracy, significantly relaxing the constraints on the silicon taper design tolerances. The taper is designed using an automated eigenmode expansion-based method, enabling efficient and manufacturing-tolerant coupling [32]. The finalized design used a 81 µm long taper with a 120 nm tip, which are shown in Figs. 2(b) and (c). A mode-field cross-section of the simulated taper is shown in Fig. 3(a) and the simulated transmission and reflection spectra are shown in Fig. 3(b). From the latter it can be seen that the optimized tapers have negligible reflections and very high simulated transmission of over 95% even for lateral misalignments of up to 500 nm.

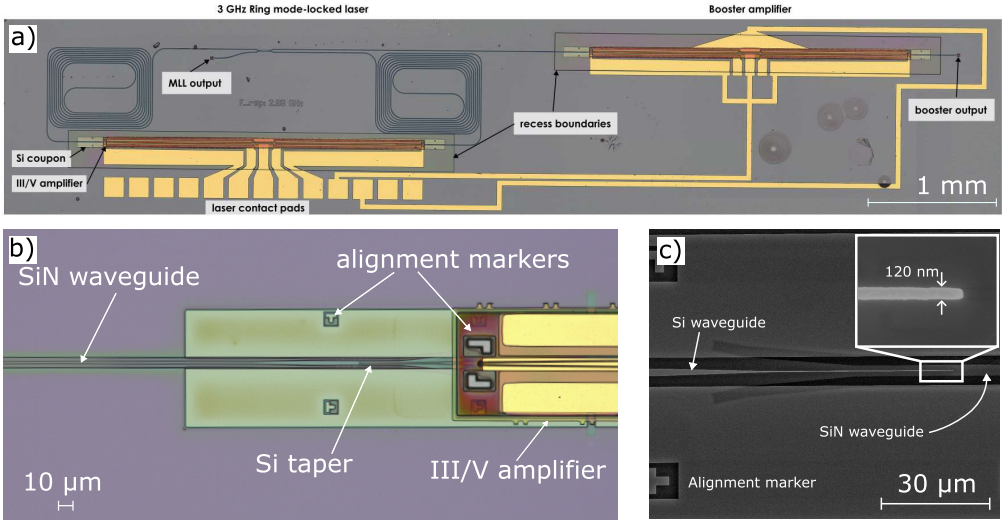

Fig. 2. (a) Microscope image of the ring mode-locked laser with booster amplifier. Locally the oxide is removed to enable heterogeneous integration closely above the SiN waveguides. (b) Zoomed-in microscope image showcasing the III/V amplifier and patterned silicon coupon on top of the SiN waveguide. (c) Scanning electron microscope (SEM) picture of the taper structure in the silicon coupon showing good alignment and accurate taper tip definition.

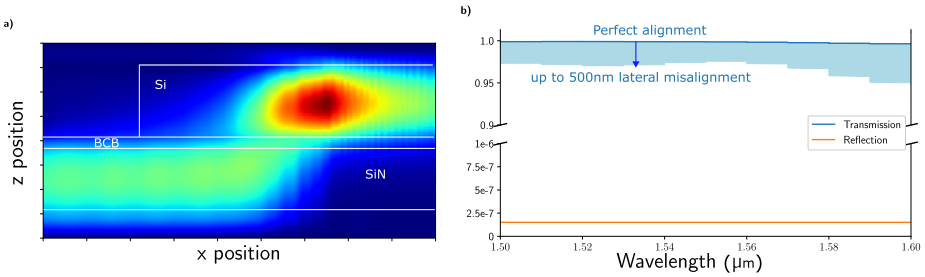

Fig. 3. (a) Mode field cross-section resulting from simulations, showing the light couples evanescently from the silicon nitride layer to the silicon layer. (b) Taper transmission spectra simulations studying the effect of lateral alignment errors.

After integration of the silicon interposer layer, the III/V amplifier can be integrated on top. The III/V amplifiers used in this work are 2.5 mm long, including a central electrically isolated

Optics EXPRESS

section of 100 µm which serves as the saturable absorber, and were obtained from the commercial III/V-labs foundry. Similar to the silicon integration, the III/V amplifiers are picked up and printed on the target sample, which is again covered in a 70-nm-thin BCB layer. The encapsulation removal and curing steps are the same, enabling to use a very standardized process flow for both steps of this two-step micro-transfer printing procedure. A schematic cross-section of the printed silicon and amplifier coupons inside of the recess can be seen in Fig. 4.

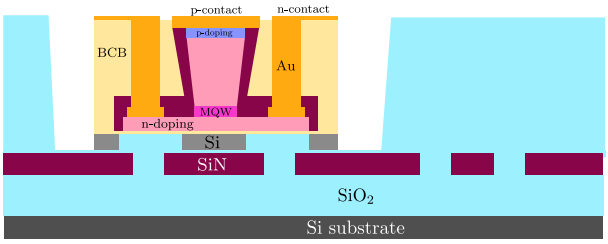

Fig. 4. Schematic representation of the cross-section of the mode-locked laser chip. Most of the chip consists of passive SiN waveguides with a thick oxide cladding. Locally the oxide is removed, to enable heterogeneous integration of the silicon coupon and III/V amplifier through micro-transfer printing.

This procedure is performed twice in parallel for this work, as besides the mode-locked laser amplifier we also include an additional booster amplifier to one of the output arms. For simplicity in this work, the exact same type of amplifier was used for the booster, but this could be changed in the future for further optimization of the gain or saturation power. As an example, an optimized amplifier design including a tapered III/V waveguide would decrease the power density and enable higher output saturation power [33]. As a result, no additional changes to the two-step transfer-printing process flow were required. A final metalization step, contacting and routing all amplifier sections and the saturable absorber to easily probed contact pads, concludes the fabrication for the demonstrated device, which is shown in Fig. 2(a).

4. Measurements

The mode-locked laser is placed on a vacuum chuck for which the temperature is kept stable at a constant 18 °C using a thermoelectric cooler (TEC), crucial to reduce the noise caused by unwanted temperature fluctuations. The mode-locked laser devices are biased using a single custom-made probe. For the mode-locked laser itself, both amplifier sections are biased using a single Keithley 2400 source measure unit, while a second unit is used to apply a reverse bias to the saturable absorber. For some of the measurements hybrid mode-locking is used to provide further control and noise reduction, for which an RF bias from a Rohde & Schwarz SMR 40 signal generator is added on top of the DC bias to the saturable absorber. As was visible in Fig. 2(a), the output from the mode-locked laser can be captured from separate grating couplers, using cleaved single mode fibers. Fiber splitters are used to characterize the different laser properties using an Anritsu MS9740A Optical Spectrum Analyzer, a Discovery DSC-R409 Photodetector (PD) connected to a Keysight N9010A Electrical Spectrum Analyzer, an HP 81531A powermeter and an APE PulseCheck autocorrelator (AC) for which the signal was pre-amplified using a Pritel pulsed Erbium Doped Fiber Amplifier (EDFA). To compare both outputs, their respective fibers were consecutively connected to the measurement tools. This measurement setup is shown schematically in Fig. 5.

Figure 6(a) shows the fiber-coupled output power as a function of the mode-locked laser amplifier bias current. The lasing threshold is ≈120 mA and average output powers up to −7 dBm are reached. When comparing this to the output of the booster amplifier, for varying bias voltages,

Optics EXPRESS

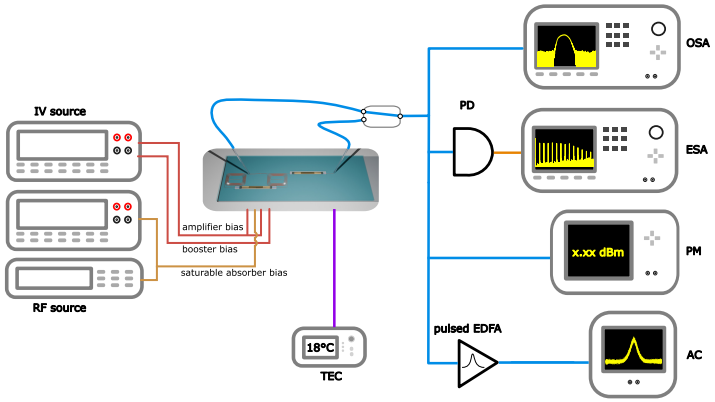

Fig. 5. Schematic visualization of the measurement setup. The measured device is kept at a constant temperature using a thermoelectric cooler (TEC). The amplifier sections are biased using current sources, while a separate source is used for applying a reverse bias to the saturable absorber, combined with an additional RF signal in case of hybrid mode-locking. Light is captured simultaneously from the mode-locked laser output and the booster output using cleaved single mode fibers, but connected to the measurement equipment one at a time. The captured light is split between an optical power meter (PM), optical spectrum analyzer (OSA), photodetector (PD) and electrical spectrum analyzer (ESA) and an autocorrelator (AC), for which the light is amplified with a pulsed erbium-doped fiber amplifier (EDFA).

it is noticeable that for lower bias voltages (<2.0 V) the amplifier is absorbing too much and no net gain is achieved. For larger bias values the output powers can be increased up to 5 dBm. When trying to push it even further (>3.5 V), the amplified spontaneous emission (ASE) from the booster amplifier becomes so large it disturbs the mode-locking operation. In Fig. 6(b) we investigated a specific mode-locking operation point for 250 mA bias current and −2.8 V reverse bias, where stable mode-locking was observed at the fundamental repetition frequency. For this operating point, the fiber-coupled output powers were observed at both outputs while sweeping the bias of the booster amplifier. For the mode-locked laser itself the output power remains stable at −5.5 dBm up until 2.0 V, after which the booster ASE starts to influence the power levels. At the highest bias values, the output power increases even further, but mode-locking operation is lost. For the booster output the power increases significantly until it saturates at 5 dBm for bias above 3.0 V.

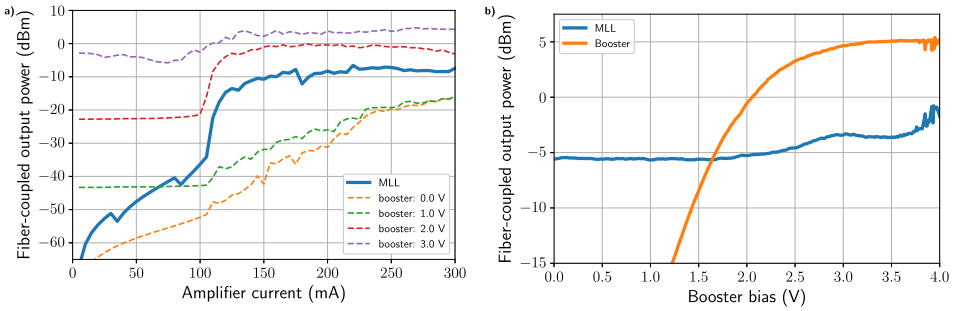

Fig. 6. (a) Fiber-coupled output power as a function of the MLL amplifier current for the MLL output and booster output, with different bias conditions of the booster amplifier. (b) Fiber-coupled output power for a specific mode-locking point (250 mA, −2.8 V) as a function of the booster amplifier bias.

Optics EXPRESS

As such the output power of the mode-locked laser was increased by 10.5 dB with the addition of this booster amplifier. The grating couplers were characterized on separate test structures, showing losses of 6 dB per coupler at 1530 nm. Correspondingly, we achieved on-chip pulse powers of 11 dBm or pulse energies of 4.2 pJ. This is a factor 2 improvement on a previous demonstration [17], where a 2 pJ pulse energy was demonstrated for a similar repetition rate mode-locked laser.

Figures 7(a) and 7(b) respectively show the optical and RF spectra for the same mode-locking operation point at 250 mA and −2.8 V, while the booster amplifier is biased at 3.0 V or 268 mA. The mode-locked laser itself shows an optical spectrum centered around 1530 nm with a 10 dB optical bandwidth of nearly 10 nm. The RF spectrum confirms fundamental mode-locking with distinct peaks at the repetition rate of 3 GHz and at the higher harmonics, with a signal-to-noise ratio of over 30 dB. On the other hand, the curves depicting the booster output show that the optical spectra can be boosted significantly, with limited change to the mode-locking spectrum aside from an increase in ASE. The small wavelength shift between the optical spectra can be attributed to both the difference in gain profiles of the SOAs, caused by bandgap shrinkage as a result of strong driving currents of the booster amplifier, as well as nonlinear effects in the amplifiers. Furthermore the RF spectra showcase that stable mode-locking is maintained. This is further exemplified in Fig. 8, for which the mode-locked laser and amplifier where operated continuously during 48 hours. We show that the passively mode-locked laser has a very stable repetition frequency with deviations smaller than ±1.0 MHz throughout the entire measurement period. The same output power was also maintained during the measurement, with only deviations due to fiber drift as a result of environmental factors. This is a strong indication of long-term stability of the repetition frequency under continuous high-optical-power operation of these micro-transfer printed mode-locked lasers.

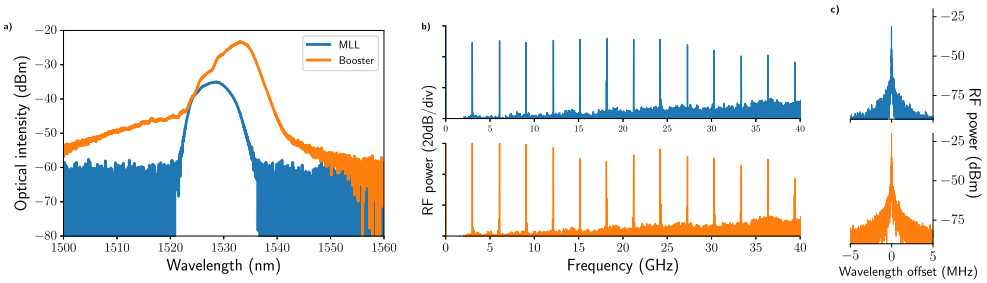

Fig. 7. (a) Optical spectrum showing the mode-locked frequency combs for the mode-locked laser and booster, while the mode-locked laser is biased at 250 mA and −2.8 V and the booster amplifier is biased with 3.0 V or 268 mA. (b) RF combs for the same conditions with a resolution bandwidth (RBW) of 100 kHz and (c) the corresponding fundamental RF lines with a RBW of 1 kHz.

Figure 9(a) shows the single-sideband phase noise (SSB-PN) for the same conditions. It confirms that the phase noise for both the mode-locked laser and the booster output is very similar and can be fitted with a 1.4 kHz Lorentzian. In both cases the phase noise can be suppressed significantly for offset frequencies below 100 kHz by applying an additional RF bias on the saturable absorber with a frequency matching the repetition rate (3 GHz). In this manner, we achieve hybrid mode-locking, in which the repetition rate is locked to an external RF source and the slow drift in cavity length or gain dynamics are compensated. From the single-sideband phase noise measurements we are able to calculate a timing jitter power spectral density of 78500 fs^2/Hz and 15.2 fs^2/Hz at a 10 kHz offset frequency for passive and hybrid mode-locking respectively. Similarly within the frequency range of 10 kHz and 1 MHz we obtain respective integrated timing jitter values of 25.7 ps and 3.5 ps. In autocorrelator measurements (Fig. 9(b))

Optics EXPRESS

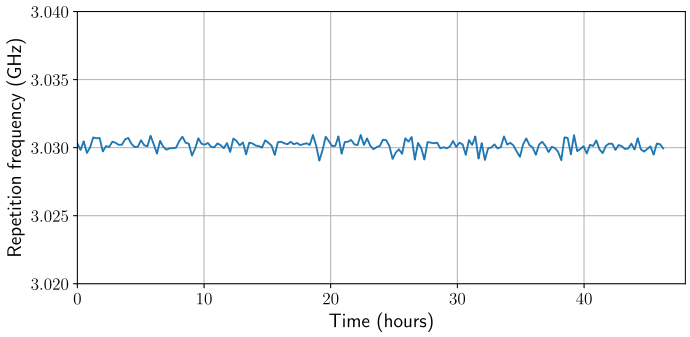

Fig. 8. Stability measurement of the repetition frequency of the mode-locked laser with booster amplifier for 48 hours continuous operation.

the pulse shapes can be seen to be very similar as well for the mode-locked laser and booster, with sech^2 deconvoluted pulse widths of 4.0 ps and 4.5 ps respectively. From these measurements we can conclude that the increase in output power comes with minimal deterioration to the noise performance of the demonstrated mode-locked laser.

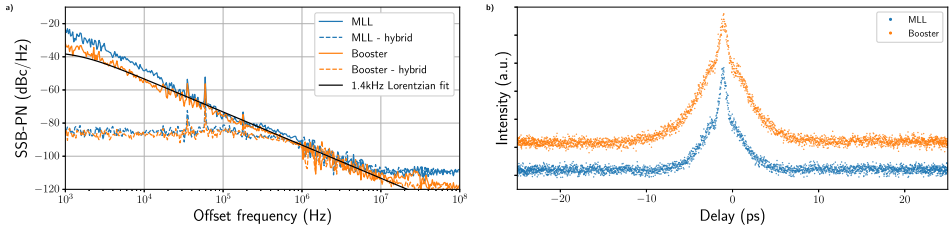

Fig. 9. (a) Single-sideband phase noise (SSB-PN) measurement of the fundamental RF lines for both the mode-locked laser and booster along with a 1.4 kHz Lorentzian fit. (b) Autocorrelation measurement of the output pulses, preamplified by a pulsed EDFA.

Comparing this result to state-of-the-art demonstrations of heterogeneous mode-locked lasers (Table 1), we show a strong improvement in terms of output power, pulse energy and optical bandwidth, as well as a reduction in pulse duration compared to other low repetition rate mode-locked lasers.

Table 1. Overview of state-of-the-art heterogeneous mode-locked lasers. Comparison is made for the repetition frequency (f_{rep}), average output power (P_{avg}), optical 10 dB bandwidth ($\Delta\lambda$), RF linewidth (δf_r), pulse energy (E_{pulse}) and the pulse duration T.

Reference	f_{rep}	P_{avg}	$\Delta\lambda$	δf_r	E_{pulse}	T
[20]	20 GHz	1.83 mW	7.14 nm	1.1 kHz	0.092 pJ	900 fs
[18]	755 MHz	0.125 mW	3.27 nm	1 Hz	0.16pJ	7.46 ps
[17]	3 GHz	5.62 mW	4 nm	400 Hz	2 pJ	8 ps
This work	3.03 GHz	12.5 mW	10 nm	1.4 kHz	4.2 pJ	4.5 ps

5. Conclusion and outlook

In this work, we demonstrate a 3 GHz repetition rate mode-locked laser, of which we can boost the output power by 10.5 dB with the addition of a booster amplifier. We fully utilize the

Optics EXPRESS

versatility of the heterogeneous integration technique called micro-transfer printing, to integrate III/V semiconductor optical amplifiers and silicon intermediate coupons. Reaching 11 dBm waveguide coupled output power is a significant improvement over previously demonstrated III/V-on-SiN mode-locked lasers. Especially for low repetition rate applications such as dual-comb spectroscopy this increase in output power could enable the next step towards fully integrated spectroscopy systems. The fiber-coupled power could be improved further by replacing the grating couplers with edge couplers, which have shown to enable coupling losses of below 1.5 dB per coupler [34]. Based on the results shown in [17] we believe that switching to a more established foundry platform should also enable us to push the limits even further. Future work could also look into optimizing the booster SOA, to potentially improve performance even further. While in this work the output power is limited by the gain saturation of the booster amplifier, ASE feedback into the mode-locked laser cavity could also become a limiting factor in the future, which could be mitigated by reducing the reflections of the output coupler, or the introduction of an optical isolator.

Funding. HORIZON EUROPE European Innovation Council (101159440).

Acknowledgment. Acknowledging the European Innovation Council Transition project MOLOKAI (Grant 101159440)

Disclosures. The authors declare no conflicts of interest.

Data availability. Data underlying the results presented in this paper are not publicly available at this time but may be obtained from the authors upon reasonable request.

References

1. S. Liu, X. Wu, D. Jung, *et al.*, "High-channel-count 20 GHz passively mode-locked quantum dot laser directly grown on Si with 41 Tbit/s transmission capacity," Optica **6**(2), 128 (2019).
2. I. Coddington, N. Newbury, and W. Swann, "Dual-comb spectroscopy," Optica **3**(4), 414 (2016).
3. N. Picqué and T. W. Hänsch, "Frequency comb spectroscopy," Nat. Photonics **13**(3), 146–157 (2019).
4. I. Coddington, W. Swann, L. Nenadovic, *et al.*, "Rapid and precise absolute distance measurements at long range," Nat. Photonics **3**(6), 351–356 (2009).
5. P. Trocha, J. N. Kemal, Q. Gaimard, *et al.*, "Ultra-fast optical ranging using quantum-dash mode-locked laser diodes," Sci. Rep. **12**(1), 1076 (2022).
6. Z. G. Lu, J. R. Liu, C. Y. Song, *et al.*, "High performance InAs/InP quantum dot 34.462-GHz C-band coherent comb laser module," Opt. Express **26**(2), 2160 (2018).
7. M. Dong, M. W. Day, H. G. Winful, *et al.*, "Quantum-well laser diodes for frequency comb spectroscopy," Opt. Express **28**(15), 21825 (2020).
8. J. J. Plant, J. T. Gopinath, B. Chann, *et al.*, "250 mW, 1.5 μm monolithic passively mode-locked slab-coupled optical waveguide laser," Tech. rep. (2006).
9. Q. Guo, B. K. Gutierrez, R. Sekine, *et al.*, "Ultrafast mode-locked laser in nanophotonic lithium niobate," Science **382**(6671), 708–713 (2023).
10. Y. Klaver, J. P. Epping, C. G. H. Roeloffzen, *et al.*, "Self-mode-locking in a high-power hybrid silicon nitride integrated laser," Opt. Lett. **47**(1), 198 (2022).
11. J. Liu, G. Huang, R. N. Wang, *et al.*, "High-yield, wafer-scale fabrication of ultralow-loss, dispersion-engineered silicon nitride photonic circuits," Nat. Commun. **12**(1), 1 (2021).
12. A. Rahim, E. Ryckeboer, A. Z. Subramanian, *et al.*, "Expanding the silicon photonics portfolio with silicon nitride photonic integrated circuits," J. Lightwave Technol. **35**(4), 639–649 (2017).
13. C. O. de Beeck, B. Haq, L. Elsinger, *et al.*, "Heterogeneous III-V on silicon nitride amplifiers and lasers via microtransfer printing," Optica **7**(5), 386 (2020).
14. C. Xiang, W. Jin, J. Guo, *et al.*, "Narrow-linewidth III-V/Si/Si 3 N 4 laser using multilayer heterogeneous integration," Optica **7**(1), 20 (2020).
15. C. Xiang, J. Guo, W. Jin, *et al.*, "High-performance lasers for fully integrated silicon nitride photonics," Nat. Commun. **12**(1), 6650 (2021).
16. B. Pan, J. Bourderionnet, V. Billault, *et al.*, "III-V-on-Si 3 N 4 widely tunable narrow-linewidth laser based on micro-transfer printing," Photonics Res. **12**(11), 2508 (2024).
17. A. Hermans, K. V. Gasse, J. Kjellman, *et al.*, "High-pulse-energy III-V-on-silicon-nitride mode-locked laser," APL Photonics **6**(9), 096102 (2021).
18. S. Cuyvers, B. Haq, C. O. de Beeck, *et al.*, "Low noise heterogeneous III-V-on-silicon-nitride mode-locked comb laser," Laser Photonics Rev. **15**(8), 2000485 (2021).
19. M. Billet, S. Cuyvers, S. Poelman, *et al.*, "Heterogeneous tunable III-V-on-silicon-nitride mode-locked laser emitting wide optical spectra," Photonics Res. **12**(3), A21 (2024).

Optics EXPRESS

20. M. L. Davenport, S. Liu, and J. E. Bowers, "Integrated heterogeneous silicon/III–V mode-locked lasers," Photonics Res. **6**(5), 468 (2018).
21. T. Vanackere, T. Vandekerckhove, L. Bogaert, *et al.*, "Heterogeneous integration of a high-speed lithium niobate modulator on silicon nitride using micro-transfer printing," APL Photonics **8**(8), 086102 (2023).
22. D. Maes, S. Lemey, G. Roelkens, *et al.*, "High-speed uni-traveling-carrier photodiodes on silicon nitride," APL Photonics **8**(1), 016104 (2023).
23. A. Hermans, K. V. Gasse, and B. Kuyken, "On-chip optical comb sources," APL Photonics **7**(10), 100901 (2022).
24. S. Latkowski, V. Moskalenko, S. Tahvili, *et al.*, "Monolithically integrated 2.5 GHz extended cavity mode-locked ring laser with intracavity phase modulators," Opt. Lett. **40**(1), 77–80 (2015).
25. S. Keyvaninia, S. Uvin, M. Tassaert, *et al.*, "Narrow-linewidth short-pulse III-V-on-silicon mode-locked lasers based on a linear and ring cavity geometry," Opt. Express **23**(3), 3221 (2015).
26. K. V. Gasse, S. Uvin, V. Moskalenko, *et al.*, "Recent advances in the photonic integration of mode-locked laser diodes," IEEE Photonics Technol. Lett. **31**(23), 1870–1873 (2019).
27. T. Reep, M. Billet, D. V. Thourhout, *et al.*, "Characterisation of a transfer-printed InP saturable absorber on a silicon platform," in *2024 Conference on Lasers and Electro-Optics Pacific Rim (CLEO-PR)*, (Optica Publishing Group, 2024), p. Fr2D3.
28. G. Roelkens, J. Zhang, L. Bogaert, *et al.*, "Present and future of micro-transfer printing for heterogeneous photonic integrated circuits," APL Photonics **9**(1), 010901 (2024).
29. D. Minemura, R. Kou, Y. Sutoh, *et al.*, "Compact magneto-optical isolator by μ-transfer printing of magneto-optical single-crystal film on silicon waveguides," Opt. Express **31**(17), 27821–27829 (2023).
30. S. Poelman, S. Cuyvers, J. D. Witte, *et al.*, "Generic heterogeneous integration process flow for commercial foundry low-index photonic platforms," *Optics InfoBase Conference Papers* pp. 6–7 (2021).
31. R. S. Cok, M. Meitl, R. Rotzoll, *et al.*, "Inorganic light-emitting diode displays using micro-transfer printing," J. Soc. Inf. Disp. **25**(10), 589–609 (2017).
32. T. Reep, S. Poelman, J. De Witte, *et al.*, "An automated design approach for fabrication-tolerant multi-segment mode couplers for heterogeneously integrated circuits," in *IEEE Photonics Benelux Annual Symposium 2024*, (2024).
33. E. Soltanian, M. Billet, A. Hermans, *et al.*, "Micro-transfer-printed III-V-on-Si semiconductor optical amplifier with 15 dBm output saturation power," in *IEEE Photonics Benelux Annual Symposium 2022*.
34. J. Fernández, R. Ba nos, D. Doménech, *et al.*, "Low-loss inverted taper edge coupler in silicon nitride," IET Optoelectron. **13**(2), 62–66 (2019).

157.193.248.10 2026-01-09 09:54:2